npj | 2D materials and applications

www.nature.com/npj2dmaterials

ARTICLE OPEN

Check for updates

# Multiferroic and ferroelectric phases revealed in 2D $Ti_3C_2T_x$ MXene film for high performance resistive data storage devices

Rabia Tahir[1], Sabeen Fatima[1], Syedah Afsheen Zahra[1], Deji Akinwande[2], Hu Li[3,4], Syed Hassan Mujtaba Jafri[5] and Syed Rizwan[1]✉

Multiferroic materials, showing simultaneous ferroelectric and ferromagnetic orders, are considered to be promising candidates for future data storage technology however, the multiferroic phenomenon in two-dimensional (2D) materials is rarely observed. We report a simple approach to observe frequency-dependent ferroelectricity and multiferroicity in 2D $Ti_3C_2T_x$ MXene film at room-temperature. To study the frequency and poling effect on ferroelectricity, we performed electric polarization vs. electric field (P-E) measurement at different frequencies, measured under zero and non-zero static magnetic fields. The results not only indicate a clear frequency dependence of electric domains owing to varying time relaxation during reversal dynamic but also showed magnetic field control of electric polarization thus, confirmed the presence of strong magneto-electric (ME) coupling at room-temperature. The existence of ME coupling was attributed to the coupling between disordered electric dipoles with local spin moments as well reduced dielectric loss after heat-treatment. Moreover, the ferroelectric $Ti_3C_2T_x$ MXene film was employed as an active layer within the resistive data storage device that showed a stable switching behavior along with improved on/off ratio in comparison to non-ferroelectric $Ti_3C_2T_x$ active layer. The unique multiferroic behavior along with ferroelectric-tuned data storage devices reported here, will help understand the intrinsic nature of 2D materials and will advance the 2D ferroelectric data storage industry.

*npj 2D Materials and Applications* (2023)7:7 ; https://doi.org/10.1038/s41699-023-00368-2

## INTRODUCTION

Materials that primarily exhibit more than one ferroic orders (ferroelectric, ferromagnetic, etc) are referred to as multiferroics (MF), offering massive technological benefits[1–3]. In MF materials, either an external electric field can control the magnetic domains and/or an external magnetic field can regulate the electric domains owing to the magnetoelectric (ME) coupling[4]. Consequently, these materials offer logic states which are used in wide spectrum of new electronics applications[5]. Hence, the data can be stored in both, the electric and magnetic states by utilizing ferroelectric polarization to write data with the help of electric field that can be read using a magnetic field[6].

Theoretically, ferroelectricity was intrinsically predicted in many 2D materials such as $In_2Se_3$, 1T-$MoS_2$ and $CuInP_2S_6$ however, experimental observation of such an effect is still rare[7]. The new emerging class of 2D materials, i.e., MXenes with the general formula of $M_{n+1}X_nT_x$ ($n = 1–3$), where M stands for early transition metal (Ti, Mo, Nb, and so on), X shows the presence of carbon or nitrogen and in some cases both of them, while $T_x$ represents the surface termination (–O, –F, –OH) groups, have attracted considerable attention due to their tremendous potential for various application[8]. Until now, MXenes offer great potential for applications such as electrochemical energy conversion (batteries, supercapacitors)[9], sensors (bio, electrochemical)[10], optical (photonics, lasers)[11] and electromagnetic shielding (EMI effect)[12].

For nano scale electronic devices, experimental and computational work was carried out in order to reveal the hidden properties such as electronic and magnetic properties of MXenes[13]. In $Sc_2CO_2$ and $Nb_2NF_2$ MXene, computational analysis confirmed the existence of ferroelectricity[14,15]. On the other hand, experimental observation on the existence of ferroelectricity and multiferroicity in $Ti_3C_2T_x$ MXene was recently reported in our previous report[16]. Also, the presence of diamagnetic-type superconductivity in $Nb_2C$ MXene with transition temperature of 12.5 K and co-existence of ferromagnetic and anti-ferromagnetic phase in $Ti_3C_2T_x$ were also reported in literature indicating that the MXene has a strong potential for various applications[17,18].

Here in this work, we have reported a detailed study on dependence of newly discovered ferroelectricity and multiferroicity in heated 2D $Ti_3C_2T_x$ MXene on factors such as frequency, electric-poling, effect of static magnetic field on ferroelectricity, etc. at room-temperature[16]. Also, both free-standing MXene (non-ferroelectric) and ferroelectric MXene (HT-$Ti_3C_2T_x$) films were employed in resistive random access memory devices that showed high on/off ratio with good reproducibility at room-temperature. We believe that our report will help understand further the multiferroic effect observed in 2D materials which are key to develop future electronic devices and next generation photovoltaic technology.

## RESULTS AND DISCUSSION

### Structural and morphological analysis

The inset of Fig. 1a shows the XRD pattern of $Ti_3C_2T_x$ MXene film measured using Dron X-ray diffractometer. The intensity of the (002) plane is the highest among all the peaks which is an indication of successful chemical etching and delamination processes[19]. After the heat treatment, the Rutile (JCPDS # 84-1286) and Anatase (JCPDS # 88-1175) phases of $TiO_2$ are clearly visible in the XRD pattern[20] shown in Fig. 1a. Figure 1b, c present

[1]Physics Characterization and Simulations Lab (PCSL), Department of Physics, School of Natural Sciences, National University of Sciences and Technology (NUST), H-12, Islamabad, Pakistan. [2]Microelectronics Research Center, The University of Texas at Austin, Austin, TX 78758, USA. [3]Shandong Technology Centre of Nanodevices and Integration, School of Microelectronics, Shandong University, Jinan 250101, China. [4]Department of Materials Science and Engineering, Uppsala University, 75121 Uppsala, Sweden. [5]Department of Electrical Engineering, Mirpur University of Science and Technology (MUST), Mirpur 10250 Azad Jammu and Kashmir, Pakistan. ✉email: syedrizwan@sns.nust.edu.pk

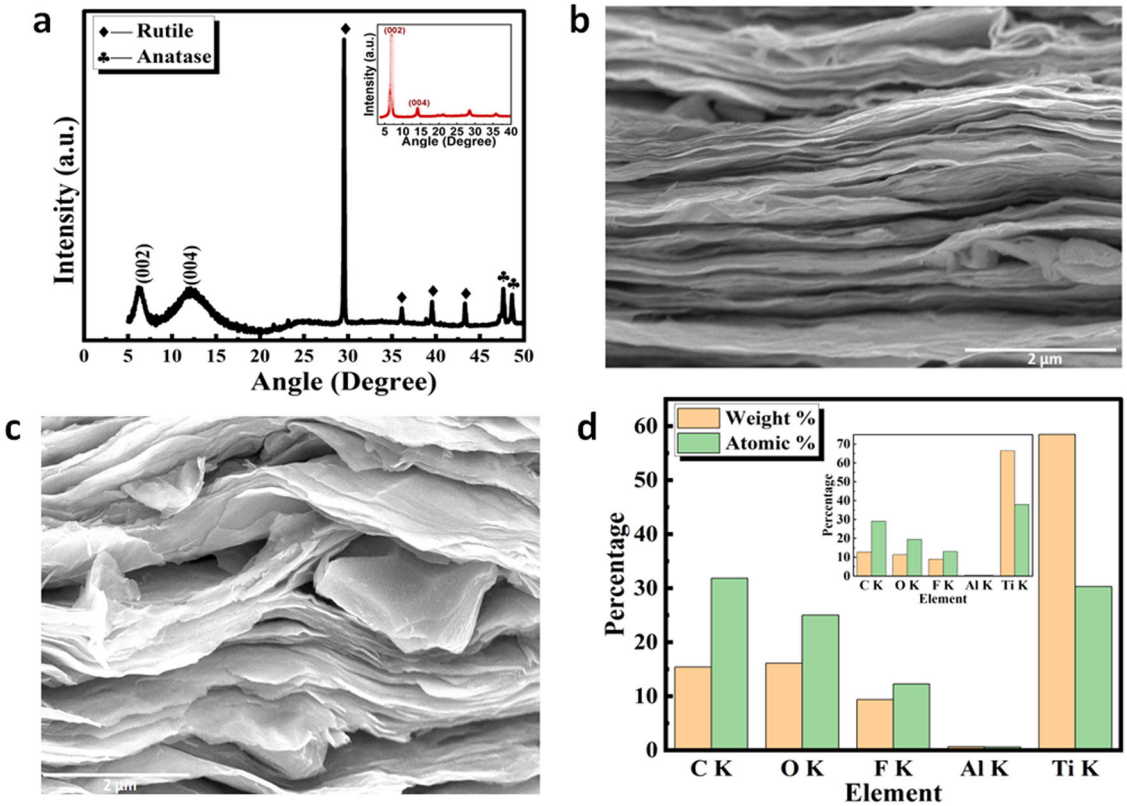


**Fig. 1 Structural and morphological characterizations. a** XRD pattern of HT-$Ti_3C_2T_x$ MXene film (inset: $Ti_3C_2T_x$ MXene film). **b** SEM image of $Ti_3C_2T_x$ MXene film. **c** SEM image of HT-$Ti_3C_2T_x$ MXene film. **d** EDX analysis of HT-$Ti_3C_2T_x$ MXene film (inset: $Ti_3C_2T_x$ MXene film).

the surface morphology images taken using scanning electron microscope (SEM) of $Ti_3C_2T_x$ MXene film and HT-$Ti_3C_2T_x$ MXene film, respectively. It is evident from the morphology that the $Ti_3C_2T_x$ MXene is successfully formed into the well-known layered structure having a clear stacking of the sheets. It is clearly seen in Fig. 1c that even after the heat treatment, the layered structure and surface morphology remained preserved. Furthermore, Fig. 1d shows the Elemental Dispersive X-ray (EDX) analysis which clearly indicates increase in oxygen percentage after heating the $Ti_3C_2T_x$ MXene film. The addition of oxygen is the cause of formation of $TiO_2$ phase in the HT-$Ti_3C_2T_x$ MXene film which is in good agreement with the XRD analysis.

In order to get information regarding the surface chemistry of our free-standing films, XPS was performed to distinguish different termination groups (i.e. -O, -OH or –F) attached to the $Ti_3C_2T_x$ film before and after heat-treatment, as shown in Fig. 2 and Supplementary Fig. 1. The XPS spectra presented here is for C *1s*, O *1s* and Ti *2p* that matches well with the previous reports[21]. Here, according to reported literature[22], the XPS spectra is explained as follows, the termination groups are assigned in Roman numerals, i.e., Moiety I represents $Ti_3C_2O_x$, Moiety II belongs to $Ti_3C_2(OH)_x$, Moiety III shows $Ti_3C_2F_x$ and Moiety IV represents $Ti_3C_2OH$-$H_2O$ referred as $H_2O_{ads}$, respectively.

In Fig. 2a, b peak at 281 eV corresponds to C-Ti-$T_x$ (I, II, III or IV), i.e., $Ti_3C_2O_x$, $Ti_3C_2$ $(OH)_x$, $Ti_3C_2F_x$ and/ or $H_2O_{ads}$ phases[23,24]. After heat treatment, the peak intensity increases which is most likely due to the increase in $O_x$ termination group. While peak at 285 eV corresponds to graphitic C–C formation[25,26]. This peak appeared because of the selective dissolution of Ti during the etching process. On the other hand, the peak at 288 eV corresponds to C–O and/ or $CH_x$ species, appearing because the surface area of samples was exposed to air resulting in the improved carbon network and increase in $TiO_2$ phase that may appear due to solvent i.e., DI water used during the delamination process[26,27]. Also, fraction of C-Ti-$T_x$ peak changes after the heat treatment which is attributed to the presence of defects in Ti-C layers[22].

In Fig. 2d, e peak at 529 eV corresponds to $TiO_2$[28,29] while other peaks at 531 eV and 532 eV correspond to the termination groups, i.e., $O_x$ and $(OH)_x$, respectively that are attached to C-Ti, resulting in the formation of $Ti_3C_2O_x$ and $Ti_3C_2(OH)_x$[28,30]. Also, peak at 532 eV corresponds to $Al_2O_3$ that appeared from the residual of Al atoms which may be present even after the etching process[30–32]. We can clearly see that the hydroxyl peak decreases after the heat treatment. The peaks at 531 eV and 532 eV are close to $TiO_2$ where O atom is near to the vacant site, i.e., at 531.5 eV which is referred to the defective $TiO_2$[22,28]. In Fig. 2g, h peak at 455 eV corresponds to Ti $2p_{3/2}$[22,23], peak at 458 corresponds to $TiO_2$[22,28,32] which is increased after heat treatment because of the oxidation, while peak at 461 eV corresponds to Ti $2p_{1/2}$[22–24]. Thus, the XPS analysis shows the existence of defective $TiO_2$ phase and defects in Ti-C layers of MXene. The role of which is further discussed below in the ferroelectric and multiferroic analysis.

## Ferroelectric analysis

Figure 3a presents P-E loops for HT-$Ti_3C_2T_x$ MXene film measured under a frequency range from 10 Hz to 1 kHz at room–temperature that clearly shows a typical ferroelectric behavior[3]. The (P-E) hysteresis loop of non-heated $Ti_3C_2T_x$ MXene film is also measured and presented in Supplementary Fig. 2 that shows a non-ferroelectric behavior. At all frequencies, the polarization curves show typical ferroelectric hysteresis loops but with varying polarization values owing to the different response of ferroelectric domains toward the applied frequencies. It can be seen from the figure that the polarization curve measured at 10 Hz is wavy that maybe perhaps due to the leakage current contributed by the free charges due to conductive surface or defects induced due to heat treatment of HT-$Ti_3C_2T_x$ MXene

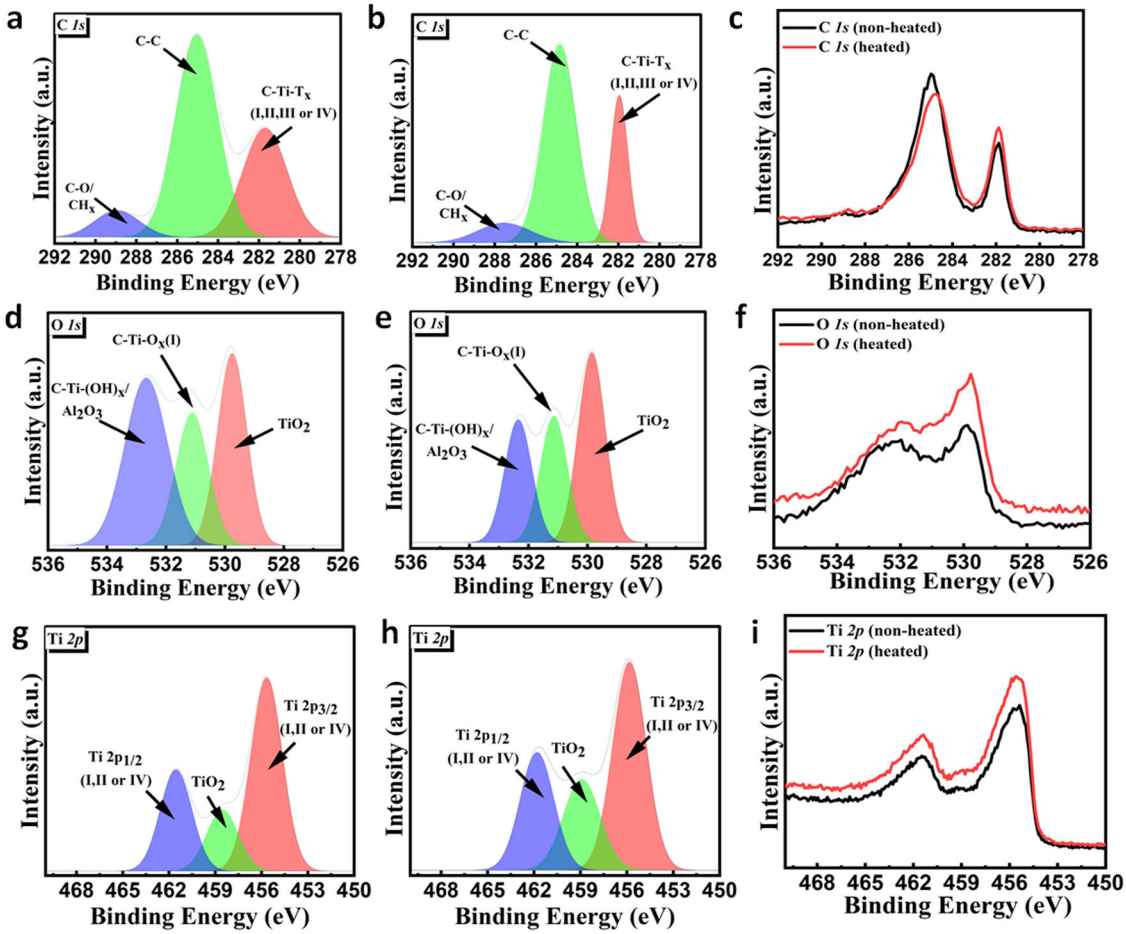


**Fig. 2 X-ray photoelectron spectroscopy analysis. a**, **b** C 1*s* region. **d**, **e** O 1*s* region. **g**, **h** Ti 2*p* region (left column $Ti_3C_2T_x$ MXene film, middle column HT-$Ti_3C_2T_x$ MXene film and right column comparison between both of them.

film[33–35]. The P-E loops retain their ferroelectric nature at all frequencies however, at relatively higher frequencies, the P-E loops become more linear keeping intact its remanence effect that could be attributed to the suppression of dipole switching[36]. One possibility of the emergency of ferroelectricity in heated sample could be the formation of $TiO_2$ layer on top of the HT-$Ti_3C_2T_x$ MXene[16]. Besides, it was also theoretically predicted that $TiO_2$ can establish ferroelectricity due to the strain-induced non-axial asymmetry[37]. Also, the Ti-O bond length plays a key role as minor perturbation could possibly induce the ferroelectricity in the system[38–40].

It is observed that the area of the P-E loop decreases with increase in frequency of the applied electric field that is attributed to the presence of free mobile charges and parasitic charges that create high concentration of charge traps[41,42]. Hence, the remanence polarization ($P_r$) is higher at low frequency due to these free charges. In Fig. 3b, the remanence polarization and saturation polarization ($P_{max}$) are shown measured at different frequencies. It can be seen that the polarization values decrease as the frequency is increased and show strong frequency dependence which is attributed to the switching response and domain relaxation of electric domains at different frequencies[41,43]. At low frequency, the ferroelectric domains switch their orientation along the field however during this process, an opposing force is faced by the domain walls just like viscosity or resistive forces. When the frequency is further increased, the domain wall switching speed also increases therefore, these forces play a key role as more field is required to surpass these opposing forces. At higher frequency, the clear degradation of polarization values can be seen owing to a few domain walls that are unable to respond to applied field[41].

## Poled and un-poled ferroelectric analysis

Figure 4 shows P-E hysteresis loops of un-poled and poled samples measured at 100 Hz. The phenomenon of poling help in the alignment of domains along the direction of poled field[3,44]. According to the reported literature, generally if the poling time is long enough, it stabilizes the orientation of electric dipoles[45]. During this phenomenon, the motion of free mobile charges helps to compensate the electric displacement which is discontinued at the interface of domain walls, thus better P-E loops can be observed under favorable poled electric field[3,46,47]. However, the electric dipoles can be aligned in the absence of interfacial charges but due to depolarization fields, these domains are relaxed to their random (original) orientations. Theoretically, the interfacial charges play an important role if the poling time exceeds beyond the relaxation time of domains. These charges help domains to fully align despite the fact that applied poled electric field is small[48].

In Fig. 4a, the $P_r$ at poled values of −0.5 kV/cm (orange color) can be attributed to the alignment of electric dipoles and the interfacial charges. Furthermore, the increase in the $P_r$ might be resulted from the poling field which favored the domain orientations by inducing the strained-domain structure[44]. The $P_r$ decreases at higher poled values of +3 kV/cm and +4 kV/cm (green and red colors) in Fig. 4b, which is close to the coercive field that may be because of the unwanted excess interfacial

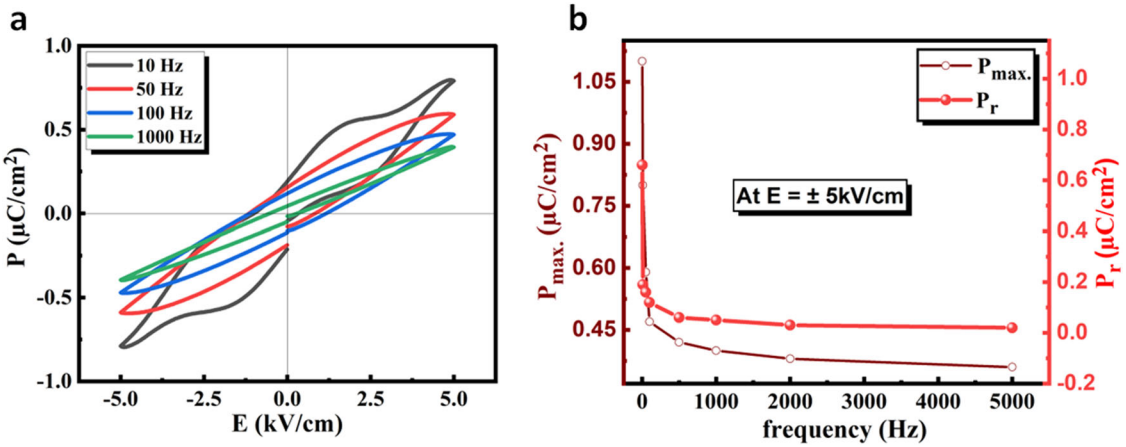


**Fig. 3 Ferroelectric effect. a** Ferroelectric hysteresis loops at different frequency ranges. **b** $P_r$, $P_{max}$ versus frequency ranges at ±5 kV/cm of HT-$Ti_3C_2T_x$ MXene film measured at room temperature.

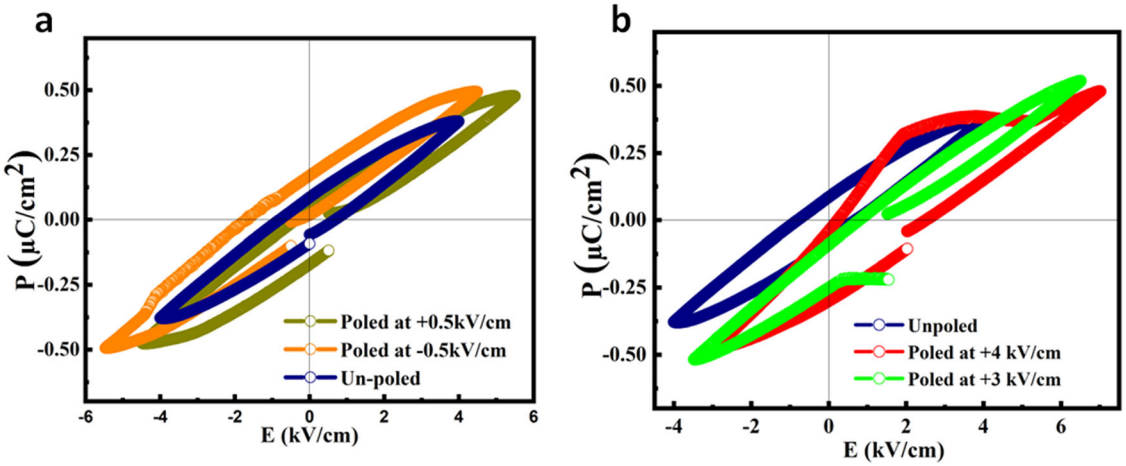


**Fig. 4 Poled and un-poled ferroelectric effect. a** P–E hysteresis loop of un-poled and poled sample at ±0.5 kV/cm electric field. **b** Un-poled and poled sample at +3 and +4 kV/cm electric field at 100 Hz frequency of HT-$Ti_3C_2T_x$ MXene film measured at room temperature.

charges which are unstable and thus, unable to respond to the poled electric field[45]. Also, the reason of slightly unsaturated P-E loops is because of conducting nature of HT-$Ti_3C_2T_x$ MXene film which exert a constant constraint on domain switching[49].

## Multiferroic and magnetoelectric effects

Figure 5a presents P-E loops measured under static magnetic fields of 0 Oe, −20 Oe, −40 Oe and −50 Oe, respectively. Also, P-E loops measured under positive static magnetic fields are shown in Supplementary Fig. 3. In order to rule out change in polarization due to the system itself, electric field in the form of continuous sine wave at frequency of 50 Hz is applied in the absence of magnetic field to get the multiple PE hysteresis loops, i.e., ~250 cycles (Supplementary Fig. 4) that showed polarization values remain consistent with almost no change due to the measuring system. The asymmetry in P-E loops in the absence and presence of magnetic fields clearly indicates the magnetic field dependence of electric polarization, opening up the possibility of tuning ferroelectric domains via magnetic field thus, confirming of the presence of strong ME coupling in HT-$Ti_3C_2T_x$ MXene film at room-temperature[50]. It is important to mention that the even a small magnetic field could change polarization by setting the magnetic spin states to develop[51]. Figure 5b shows the magnetoelectric coupling versus applied magnetic field measured at 5 Hz. Various models are suggested to explain the presence of ME coupling however, the spin-orbital coupling is more suitable owing to the coupling between disordered electric dipoles with local spin moments[52–54]. In addition, the spin-pair correspondence between ME coupling and neighboring spins causes the existence of negative value of ME coefficient[3,55] as shown in Fig. 5b. The presence of different phases of $TiO_2$ and $Ti_3C_2/TiO_2$ may further cause the ferromagnetic effect at room-temperature[16,56]. According to reported literature[3], the magnetic field dependence of magnetostriction causing initially an increase in ME coefficient at increasing magnetic field however, further increase in the field results in degradation of ME coefficient[57]. Also, when the magnetic field is applied, the domains start to grow which causes increase in ME coefficient however after the saturation point of domain growth, further increase in magnetic field causes the deformation of domains and decreases ME coupling. This is due to the direct dependence of deformation of domains and ME effect on each other[58–60]. Furthermore, the large and small peaks observed around 100 Oe and 150 Oe are possibly due to the existence of different phases ($TiO_2$ and $Ti_3C_2/TiO_2$).

## Memory device testing and analysis

Figure 6a shows the basic trilayer schematic of the memory device consisting of rGO/MXene/Pd structure consisting of

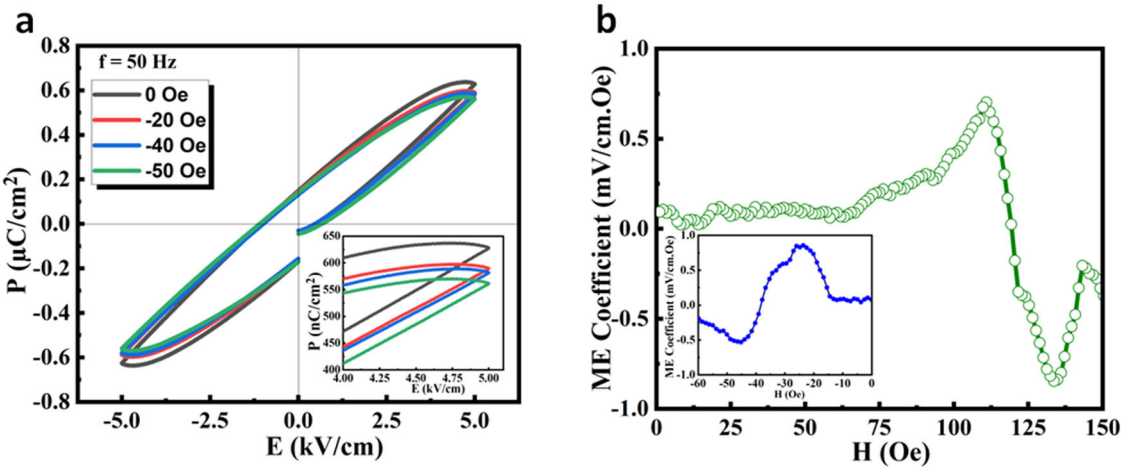


**Fig. 5 Multiferroic and magnetoelectric effect. a** The P–E loop in static magnetic field at 50 Hz frequency. **b** The magnetoelectric coefficient versus applied DC magnetic field at 5 Hz frequency of HT-$Ti_3C_2T_x$ MXene film measured at room temperature.

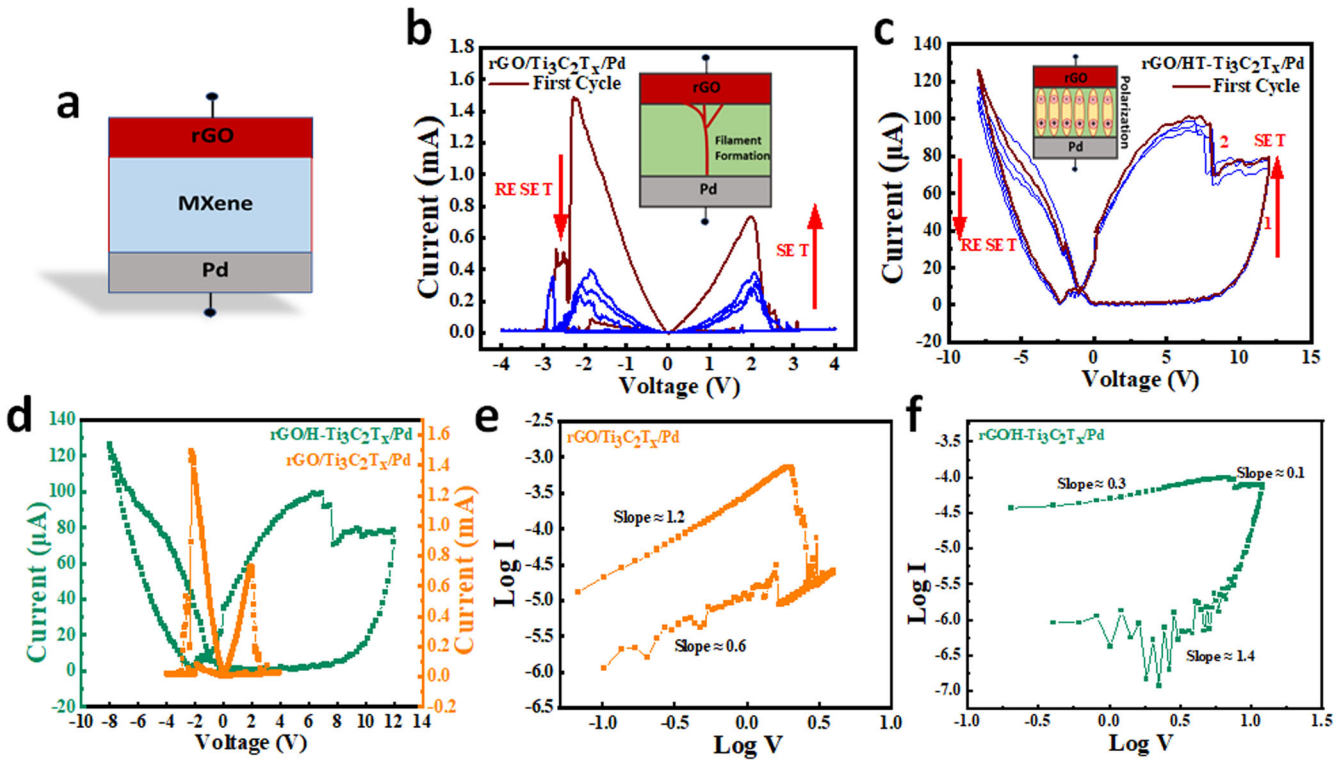


**Fig. 6 Memory device testing. a** Schematic representation of trilayer memory device. **b** Resistive switching behavior of rGO/$Ti_3C_2T_x$/Pd. **c** Resistive switching behavior of rGO/HT-$Ti_3C_2T_x$/Pd. **d** First cycle of both rGO/$Ti_3C_2T_x$/Pd and rGO/HT-$Ti_3C_2T_x$/Pd memory devices. **e** Double logarithmic graph of rGO/$Ti_3C_2T_x$/Pd. **f** rGO/HT-$Ti_3C_2T_x$/Pd memory device.

non-ferroelectric $Ti_3C_2T_x$ MXene film (device 1) and ferroelectric HT-$Ti_3C_2T_x$ MXene film (device 2) as the middle active layer. This device design is expected to reveal the proximity effect of a ferroelectric layer on the device performance. In Fig. 6b, c first 4 switching cycles of both the devices are presented, respectively. Both the devices showed bipolar resistive switching with positive SET and negative RESET states. In rGO/$Ti_3C_2T_x$/Pd device, the bias of ±4 V is applied to observe the switching behavior for which, SET state is achieved at ~2.5 V and the RESET state at 2.3 V. The maximum current passing through the device is higher in both SET and RESET states for the first switching cycle. After that, the switching behavior becomes approximately symmetric for both positive as well as negative bias polarities. In rGO/HT-$Ti_3C_2T_x$ /Pd device, a positive bias of +12 V is applied to achieve SET state while −8 V is applied to achieve the RESET state of the memory device. Also, there is no difference in device behavior for first and last switching cycle that shows good stability and reproducibility.

Figure 6d shows the comparison of the very first cycle of both, rGO/$Ti_3C_2T_x$/Pd and rGO/HT-$Ti_3C_2T_x$/Pd memory devices. In rGO/$Ti_3C_2T_x$/Pd, the maximum current in SET state is lower in comparison to RESET state which may be attributed to the more carrier conduction. As a result of which, the charge carriers (absorbed during low resistance state (LRS) from MXene middle

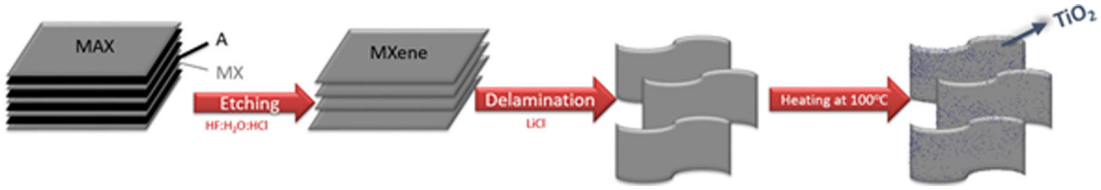


**Fig. 7 Schematics of experimentation.** Synthesis and oxidation of free-standing $Ti_3C_2T_x$ MXene film to get HT-$Ti_3C_2T_x$ MXene film.

layer) along with trapped electrons inside the rGO layers[61] will be desorbed and travel along the conducting filament, providing more current at negative bias. In rGO/HT-$Ti_3C_2T_x$/Pd device, there is zero current at zero volt initially however on increasing the bias voltage along with the switching carrier, the polar domains also help in establishing the SET states. The non-zero current at zero volt may be attributed to the remanence effect of the ferroelectric domains of the HT-$Ti_3C_2T_x$ active layer. On reversing the voltage, RESET state was achieved with rupturing of carrier conduction filament. In RESET state, the zero current was obtained at around −2.3 V. This asymmetric switching behavior of the device can be related to random growth and nucleation of the ferroelectric polar domains inside the device[62]. MXene ($Ti_3C_2T_x$), along with small terminations, can act as a dielectric medium but with its conducting nature, it may also possess leakage current as a result of the dielectric loss[63]. This loss may be attributed to the decrease in current for rGO/$Ti_3C_2T_x$/Pd device in second to last switching cycle. This loss could be minimized by providing coupling with the ferroelectric domains[64]. Here, with the heat-treatment, MXene itself converted into a ferroelectric medium which, upon using as the middle layer within rGO/HT-$Ti_3C_2T_x$/Pd memory device, provided an overall improved switching behavior with better on/off ratio. In both the devices, the SET switching voltages are in compliment with the electric field values applied to MXene for polarization. The double logarithmic graphs of both the devices are also presented in Fig. 6e, f for illustration of the conduction mechanism. The slope values equal to 1 support Ohmic conduction, while the values >1 support charge trapped SCLC conduction mechanism. Our report presents an in-depth analysis of very recent report on the multiferroic effect in MXene which open-up new avenues for 2D layered materials based future data storage devices.

In summary, the free-standing $Ti_3C_2T_x$ MXene film was synthesized and heat-treated at optimized temperature. To investigate the existence of ferroelectricity at room-temperature, polarization vs. electric field (P-E) loops were measured at different frequencies that showed typical ferroelectric behavior at all frequencies. Furthermore, the magneto-electric coupling was confirmed by asymmetric P-E loops measured under static magnetic fields along with ME coupling measurement. The reason that polarization values are strongly dependent on frequency is essentially because of switching of the domain walls and their varying relaxation times at different frequencies. We suggest that the coupling between different ferric orders caused the existence of ME coefficient thus, revealing the multiferroic nature of the HT-$Ti_3C_2T_x$ MXene film at room-temperature. Furthermore, the memristive device testing, employing the ferroelectric active layer, also showed a clear ferroelectric proximity-induced switching behavior with improved switching behavior and minimized dielectric loss.

## METHODS

### Material synthesis and characterization

Firstly, the $Ti_3C_2T_x$ MXene was prepared by selective etching of Al from $Ti_3AlC_2$ MAX phase. The process of etching was started by slowly adding 1 g of $Ti_3AlC_2$ MAX powder in Teflon-lined vessel containing 1:3:5 volume ratio of 48 wt % of hydrofluoric acid (HF, 1 ml), de-ionized water (DI water, 3 ml) and 37 wt% of hydrochloric acid (HCl, 5 ml), respectively under constant stirring at 450 rpm and 35 °C. After 24 h, the obtained solution was washed with DI water until pH ≈ 7 is obtained. After every wash, the supernatant was discarded in order to get rid of any impurity. The obtained $Ti_3C_2T_x$ MXene was then filtered and dried overnight in vacuum oven at room-temperature. For delamination, $Ti_3C_2T_x$ MXene was dispersed in lithium chloride (LiCl, 99%) and DI water (20 ml) and was continuously manually mixed for about 10 min. The solution was left for 24 h under constant stirring of 300 rpm. After this process, the intercalated solution was dispersed in DI water and centrifuged for 5 min at 3500 rpm. A stable colloidal MXene solution was obtained after repeated centrifugation to completely remove the supernatant and a clay-like sediment was obtained. The sediment was then diluted with DI water and centrifuged for 30 min at 3500 rpm. Once done, the obtained supernatant was vacuum filtered with the help of Celgard membrane in order to form the free-standing film. The obtained free-standing $Ti_3C_2T_x$ MXene was heated at 100 °C under ambient environment in order to get optimum oxidation of our sample[16,65]. The synthesis process of free-standing HT-$Ti_3C_2T_x$ MXene film is shown in Fig. 7.

In order to verify successful synthesis of free-standing $Ti_3C_2T_x$ MXene film and to observe the effect of heat treatment on structure and chemistry of MXene, X-ray diffraction (XRD) and X-ray Photoelectron Spectroscopy (XPS) were used and the results are presented in Figs. 1, 2 respectively. The polarization vs electric field (P-E) loops at different frequencies were also tested to observe the ferroelectric behavior of our material. Also, the P-E loops were subjected to DC biasing (poled) to see the response of electric domains of HT-$Ti_3C_2T_x$ MXene film to the poling. Furthermore, P-E loops were subjected to different static magnetic fields so that the response of magnetic domains in ferroelectric MXene could be explored at room-temperature. In order to confirm the presence of multiferroic nature of HT-$Ti_3C_2T_x$ MXene film, the magnetoelectric coefficient was also measured. Moreover, the ferroelectric MXene was employed as active layer in resistive data storage device so that ferroelectric-controlled resistive switching could be realized.

### Ferroelectric testing of free-standing MXene film

To test the frequency-dependent ferroelectric and multiferroic behavior of HT-$Ti_3C_2T_x$ MXene film, the Precision Multiferroic II (Precision Material Analyzer) by Radiant Technologies Inc. tester was used at room-temperature. The HT-$Ti_3C_2T_x$ MXene film of thickness of about 20 µm, having dimension of 0.2 × 0.4 cm, was mounted on to the ferroelectric test stage to observe the ferroelectric response.

### Device fabrication

For fabrication of the memory device, the bottom electrode palladium (Pd) metal was deposited over the $SiO_2$/Si substrate along with the non-ferroelectric MXene ($Ti_3C_2T_x$) and heat-treated ferroelectric MXene (HT-$Ti_3C_2T_x$) films were employed as middle insulating layers in two separate devices followed by spin-coated rGO top metal electrode to complete the trilayer rGO/MXene/Pd memory device scheme.

## DATA AVAILABILITY

The data will be available on demand.

Received: 30 September 2022; Accepted: 13 January 2023;
Published online: 03 February 2023

## REFERENCES

1. Eerenstein, W., Mathur, N. D. & Scott, J. F. Multiferroic and magnetoelectric materials. *Nature* **442**, 759–765 (2006).
2. Zhou, Y. et al. Frequency and field dependence of magnetoelectric coupling in multiferroic particulate composites. *Eur. Phys. J. Appl. Phys.* **56**, 30201 (2011).
3. Bhoi, K. et al. Unravelling the nature of magneto-electric coupling in room temperature multiferroic particulate ($PbFe_{0.5}Nb_{0.5}O_3$)–($Co_{0.6}Zn_{0.4}Fe_{1.7}Mn_{0.3}O_4$) composites. *Sci. Rep.* **11**, 1–17 (2021).
4. Ortega, N., Kumar, A., Scott, J. F. & Katiyar, R. S. Multifunctional magnetoelectric materials for device applications. *J. Phys.: Condens. Matter* **27**, 504002 (2015).
5. Ramesh, R. & Spaldin, N. A. Multiferroics: progress and prospects in thin films. *Nat. Mater.* **6**, 21–29 (2007).
6. Wood,V. E. & Austin, A. E. in *Magnetoelectric Interaction Phenomena in Crystals* (Freeman, A. J. & Schmid, H.) 181–194 (Gordon and Breach Science Publishers, Newark, New York, 1975).
7. Guan, Z. et al. Recent progress in two-dimensional ferroelectric materials. *Adv. Electron. Mater.* **6**, 1900818 (2020).
8. Gogotsi, Y. & Anasori, B. The rise of MXenes. *ACS Nano* **13**, 8491–8494 (2019).
9. Pang, J. et al. Applications of 2D MXenes in energy conversion and storage systems. *Chem. Soc. Rev.* **48**, 72–133 (2019).
10. Szuplewska, A. et al. Future applications of MXenes in biotechnology, nanomedicine, and sensors. *Trends Biotechnol.* **38**, 264–279 (2020).
11. Fu, B. et al. MXenes: Synthesis, optical properties, and applications in ultrafast photonics. *Small* **17**, 2006054 (2021).
12. Shahzad, F. et al. Electromagnetic interference shielding with 2D transition metal carbides (MXenes). *Science* **353**, 1137–1140 (2016).
13. Li, Y, et al. Insights into electronic and magnetic properties of MXenes: from a fundamental perspective. *Sustain. Mater. Technol.* **34**, e00516 (2022).
14. Chandrasekaran, A., Mishra, A. & Singh, A. K. Ferroelectricity, antiferroelectricity, and ultrathin 2D electron/hole gas in multifunctional monolayer MXene. *Nano Lett.* **17**, 3290–3296 (2017).
15. Wijethunge, D., Zhang, L. & Du, A. Prediction of two-dimensional ferroelectric metal Mxenes. *J. Mater. Chem. C* **9**, 11343–11348 (2021).
16. Tahir, R., Zahra, S. A., Naeem, U., Akinwande, D. & Rizwan, S. First observation on emergence of strong room-temperature ferroelectricity and multiferroicity in 2D-$Ti_3C_2T_x$ free-standing MXene film. *RSC Adv.* **12**, 24571–24578 (2022).
17. Babar, Z. U. et al. Peculiar magnetic behaviour and Meissner effect in two-dimensional layered $Nb_2C$ MXene. *2D Mater.* **7**, 035012 (2020).
18. Iqbal, M. et al. Co-existence of magnetic phases in two-dimensional MXene. *Mater. Today Chem.* **16**, 100271 (2020).
19. Shuck, C. E. et al. Scalable synthesis of $Ti_3C_2T_x$ mxene. *Adv. Eng. Mater.* **22**, 1901241 (2020).
20. Senapati, K., Kamal, C., Borgohain & Phukan, P. $CoFe_2O_4$-ZnS nanocomposite: a magnetically recyclable photocatalyst. *Catal. Sci. Technol.* **2**, 2361–2366 (2012).
21. Cao, Y. et al. Enhanced thermal properties of poly (vinylidene fluoride) composites with ultrathin nanosheets of MXene. *RSC Adv.* **7**, 20494–20501 (2017).
22. Halim, J. et al. X-ray photoelectron spectroscopy of select multi-layered transition metal carbides (MXenes). *Appl. Surf. Sci.* **362**, 406–417 (2016).
23. Schier, V., Michel, H.-J. & Halbritter, J. ARXPS-analysis of sputtered TiC, SiC and $Ti_{0.5}Si_{0.5}C$ layers. *Fresenius' J. Anal. Chem.* **346**, 227–232 (1993).
24. Myhra, S., Crossley, J. A. A. & Barsoum, M. W. Crystal-chemistry of the $Ti_3AlC_2$ and $Ti_4AlN_3$ layered carbide/nitride phases—characterization by XPS. *J. Phys. Chem. Solids* **62**, 811–817 (2001).
25. Lukatskaya, M. R. et al. Room-temperature carbide-derived carbon synthesis by electrochemical etching of MAX phases. *Angew. Chem.* **126**, 4977–4980 (2014).
26. Jayaweera, P. M., Quah, E. L. & Idriss, H. Photoreaction of ethanol on $TiO_2$ (110) single-crystal surface. *J. Phys. Chem. C* **111**, 1764–1769 (2007).
27. Sultana, T. et al. XPS analysis of laser transmission micro-joint between poly (vinylidene fluoride) and titanium. *Appl. Surf. Sci.* **255**, 2569–2573 (2008).
28. Diebold, U. & Madey, T. E. $TiO_2$ by XPS. *Surf. Sci. Spectra* **4**, 227–231 (1996).
29. Beamson, G. & Briggs, D. *High resolution XPS of organic polymers* (The Scienta ESCA 300 Database, Wiley, Chichester [England]; New York, 1992).
30. Ernst, K. -H., Grman, D., Hauert, R. & Holländer, E. Fluorine-Induced corrosion of aluminium microchip bond pads: An XPS and AES analysis. *Surf. interface Anal.* **21**, 691–696 (1994).
31. Popova, I., Zhukov, V. & Yates, J. T. Depth-dependent electrical impedance distribution in $Al_2O_3$ films on Al (111) detection of an inner barrier layer. *Langmuir* **16**, 10309–10314 (2000).
32. Santerre, F., El Khakani, M. A., Chaker, M. & Dodelet, J. P. Properties of TiC thin films grown by pulsed laser deposition. *Appl. Surf. Sci.* **148**, 24–33 (1999).
33. Prajapati, P. & Singh, A. K. Band gap tuning of ferroelectric $PbTiO_3$ by Mo doping. *J. Mater. Sci.: Mater. Electron.* **33**, 2550–2565 (2022).
34. Merz, W. J. Double hysteresis loop of $BaTiO_3$ at the Curie Point. *Phys. Rev.* **91**, 513 (1953).
35. Yun, S. Double Hysteresis Loop in $BaTiO_3$-Based Ferroelectric Ceramics" In Ferroelectrics: Characterization and Modeling, edited by Mickaël Lallart. London: IntechOpen. https://doi.org/10.5772/16502 (2011).
36. Mai, M., Leschhorn, A. & Kliem, H. The field and temperature dependence of hysteresis loops in P (VDF–TrFE) copolymer films. *Phys. B: Condens. Matter* **456**, 306–311 (2015).
37. Liu, Y. et al. Negative pressure induced ferroelectric phase transition in rutile $TiO_2$. *J. Phys.: Condens. Matter* **21**, 275901 (2009).
38. Barrett, J. H. Dielectric constant in perovskite type crystals. *Phys. Rev.* **86**, 118 (1952).
39. Ang, C., Yu, Z., Vilarinho, P. M. & Baptista, J. L. Bi: $SrTiO_3$: a quantum ferroelectric and a relaxor. *Phys. Rev. B* **57**, 7403 (1998).
40. Mitsui, T. & Westphal, W. B. Dielectric and X-Ray Studies of $Ca_x Ba_{1-x}Ti_3$ and $Ca_x Sr_{1-x} TiO_3$. *Phys. Rev.* **124**, 1354 (1961).
41. Hussain, A., Sinha, N., Joseph, A. J., Goel, S. & Kumar, B. Ferroelectric Sb-doped PMN-PT crystal: high electromechanical response with true-remanent polarization and resistive leakage analyses. *J. Mater. Sci.: Mater. Electron.* **29**, 19567–19577 (2018).
42. Mukherjee, A., Basu, S., Manna, P. K., Yusuf, S. M. & Pal, M. Giant magnetodielectric and enhanced multiferroic properties of Sm doped bismuth ferrite nanoparticles. *J. Mater. Chem. C* **2**, 5885–5891 (2014).
43. Scott, J. F. Models for the frequency dependence of coercive field and the size dependence of remanent polarization in ferroelectric thin films. *Integr. Ferroelectr.* **12**, 71–81 (1996).
44. Rachakom, A., Jiansirisomboon, S. & Watcharapasorn, A. Effect of poling on piezoelectric and ferroelectric properties of $Bi_{0.5}Na_{0.5}Ti_{1-x}Zr_xO_3$ ceramics. *J. Electroceram.* **33**, 105–110 (2014).
45. Kwok, K., Wing, S. T., Lau, C. K., Wong & Shin, F. G. Effects of electrical conductivity on poling of ferroelectric composites. *J. Phys. D: Appl. Phys.* **40**, 6818 (2007).
46. Mohanty, H. S. et al. Structural transformations and physical properties of $(1-x)Na_{0.5}Bi_{0.5}TiO_3-xBaTiO_3$ solid solutions near a morphotropic phase boundary. *J. Phys.: Condens. Matter* **31**, 075401 (2018).
47. Borkar, H., Tomar, M., Gupta, V., Scott, J. F. & Kumar, A. Anomalous change in leakage and displacement currents after electrical poling on lead-free ferroelectric ceramics. *Appl. Phys. Lett.* **107**, 122904 (2015).
48. Kwok, K. W., Wong, C. K., Zeng, R. & Shin, F. G. AC Poling study of lead zirconate titanate/vinylidene fluoride-trifluoroethylene composites. *Appl. Phys. A* **81**, 217–222 (2005).
49. Chowdhury, U., Goswami, S., Bhattacharya, D., Midya, A. & Mandal, P. Determination of intrinsic ferroelectric polarization in lossy improper ferroelectric systems. *Appl. Phys. Lett.* **109**, 092902 (2016).
50. Mandal, M., Chatterjee, S. & Palkar, V. R. Multifunctional behavior of ZnO supported $Bi_{1-x}Dy_xFeO_3$ nanorods. *J. Appl. Phys.* **110**, 054313 (2011).
51. Ruff, A., Loidl, A. & Krohns, S. Multiferroic hysteresis loop. *Materials* **10**, 1318 (2017).
52. Shah, J. & Kotnala, R. K. Induced magnetism and magnetoelectric coupling in ferroelectric $BaTiO_3$ by Cr-doping synthesized by a facile chemical route. *J. Mater. Chem. A* **1**, 8601–8608 (2013).
53. Ortega, N., Kumar, A., Scott, J. F. & Katiyar, R. S. Multifunctional magnetoelectric materials for device applications. *J. Phys.: Condens. Matter* **27**, 504002 (2015).
54. Hemberger, J. et al. Relaxor ferroelectricity and colossal magnetocapacitive coupling in ferromagnetic $CdCr_2 S_4$. *Nature* **434**, 364–367 (2005).
55. Pradhan, D. K. et al. Room temperature multiferroic properties of Pb $(Fe_{0.5}Nb_{0.5})O_3$–$Co_{0.56}Zn_{0.35}Fe_2O_4$ composites. *J. Appl. Phys.* **114**, 234106 (2013).
56. Wei, X. et al. Magnetism of TiO and $TiO_2$ nanoclusters. *J. Appl. Phys.* **105**, 07C517 (2009).
57. Pradhan, D. K., Chowdhury, R. N. P. & Nath, T. K. Magnetoelectric properties of $PbZr_{0.53}Ti_{0.47}O_3$–$Ni_{0.65}Zn_{0.35}Fe_2O_4$ multiferroic nanocomposites. *Appl. Nanosci.* **2**, 261–273 (2012).
58. Van Suchtelen, J. Product properties: a new application of composite materials. *Phillips Res. Rep.* **27**, 28–37 (1972).
59. Fiebig, M. Revival of the magnetoelectric effect. *J. Phys. D: Appl. Phys.* **38**, R123 (2005).
60. Gualdi, A. J. et al. Understanding the dynamic magnetization process for the magnetoelectric effect in multiferroic composites. *J. Appl. Phys.* **119**, 124110 (2016).
61. Fatima, S., Bin, X., Mohammad, M. A., Akinwande, D. & Rizwan, S. Graphene and MXene based free-standing carbon memristors for flexible 2d memory applications. *Adv. Electron. Mater.* **8**, 2100549 (2021).

62. Qian, M., Fina, I., Sánchez, F. & Fontcuberta, J. Asymmetric resistive switching dynamics in $BaTiO_3$ tunnel junctions. *Adv. Electron. Mater.* **5**, 1800407 (2019).
63. Tu, S., Jiang, Q., Zhang, X. & Alshareef, H. N. Large dielectric constant enhancement in MXene percolative polymer composites. *ACS Nano* **12**, 3369–3377 (2018).
64. Ghosh, S. K. et al. Ferroelectric multilayer nanocomposites with polarization and stress concentration structures for enhanced triboelectric performances. *ACS Nano* **14**, 7101–7110 (2020).
65. Low, J., Zhang, L., Tong, T., Shen, B. & Yu, J. $TiO_2$/MXene $Ti_3C_2$ composite with excellent photocatalytic $CO_2$ reduction activity. *J. Catal.* **361**, 255–266 (2018).

## ACKNOWLEDGEMENTS

The authors thank the Higher Education Commission (HEC) of Pakistan for providing research funding under the Project No.: 20-14784/NRPU/R&D/HEC/2021. The authors also acknowledge the financial support from Shandong Provincial Natural Science Foundation (Grant No.: ZR2021QE148), Shandong Provincial Natural Science Foundation for Excellent Young Scientists Fund Program (Overseas) (Grant No.: 2022HWYQ-060).

## AUTHOR CONTRIBUTIONS

R.T. performed testing, analysis and write-up of results, S.F. performed device fabrication, memory testing and analyzing, S.A.Z. helped in materials synthesis, D.A. helped understand the memory phenomena, H.L. and S.H.M.J. helped in XPS testing and analysis and S.R. conceived the idea and supervised the project.

## COMPETING INTERESTS

The authors declare no competing interests.

## ADDITIONAL INFORMATION

**Supplementary information** The online version contains supplementary material available at https://doi.org/10.1038/s41699-023-00368-2.

**Correspondence** and requests for materials should be addressed to Syed Rizwan.

**Reprints and permission information** is available at http://www.nature.com/reprints

**Publisher's note** Springer Nature remains neutral with regard to jurisdictional claims in published maps and institutional affiliations.